Aalto University

Varglund, I.; Järvelä, E.; Ciroi, S.; Berton, M.; Congiu, E.; Lähteenmäki, A.; Di Mille, F.

A host galaxy study of southern narrow-line Seyfert 1 galaxies

Astronomy & Astrophysics

A host galaxy study of southern narrow-line Seyfert 1 galaxies

I. Varglund[1,2] , E. Järvelä[3,4][⋆], S. Ciroi[5], M. Berton[6], E. Congiu[6], A. Lähteenmäki[1,2], and F. Di Mille[7]

[1] Aalto University Metsähovi Radio Observatory, Metsähovintie 114, 02540 Kylmälä, Finland
e-mail: irene.varglund@aalto.fi
[2] Aalto University Department of Electronics and Nanoengineering, PO Box 15500, 00076 Aalto, Finland
[3] European Space Agency (ESA), European Space Astronomy Centre (ESAC), Camino Bajo del Castillo s/n, 28692 Villanueva de la Cañada, Madrid, Spain
[4] Homer L. Dodge Department of Physics and Astronomy, The University of Oklahoma, 440 W. Brooks St., Norman, OK 73019, USA
[5] Dipartimento di Fisica e Astronomia "G. Galilei", Universitá di Padova, Vicolo dell'Osservatorio 3, 35122 Padova, Italy
[6] European Southern Observatory (ESO), Alonso de Córdova 3107, Casilla 19, Santiago 19001, Chile
[7] Las Campanas Observatory, Carnegie Observatories, Colina El Pino, Casilla 601, La Serena, Chile

ABSTRACT

We studied seven nearby narrow-line Seyfert 1 (NLS1) galaxies in J and Ks bands with redshifts varying from 0.019 to 0.092. This is the first multi-source study targeting the hosts of southern NLS1 galaxies. Our data were obtained with the FourStar instrument of the 6.5 m *Magellan Baade* telescope at the Las Campanas Observatory (Chile). The aim of our study is to determine the host galaxy morphologies of these sources by using GALFIT. We were able to model six out of the seven sources reliably. Our conclusion is that all of the reliably modelled sources are disk-like galaxies, either spirals or lenticulars. None of these sources present an elliptical morphology. Our findings are in agreement with the hypothesis that disk-like galaxies are the main host of jetted NLS1 galaxies. Taking advantage of observations in two bands, we also produced a $J - Ks$ colour map of each source. Five of the six colour maps show significant dust extinction near the core of the galaxy – a feature often seen in gamma-ray-detected jetted NLS1 galaxies, and interpreted to be a consequence of a past minor merger.

Key words. galaxies: active – galaxies: Seyfert – galaxies: structure – infrared: galaxies

1. Introduction

Narrow-line Seyfert 1 (NLS1) galaxies (Osterbrock & Pogge 1985) are a class of peculiar active galactic nuclei (AGN). The full width at half maximum (FWHM) of Hβ is, by definition, less than $2000 \, \mathrm{km \, s^{-1}}$ (Goodrich 1989). This class is often characterised by its unique optical spectral line features. One of the most common identifiers of NLS1 galaxies is the faint [O III] emission with respect to Hβ (S([O III]λ5007)/S(Hβ) < 3; Osterbrock & Pogge 1985). Though this is not the case for all NLS1 galaxies, a considerable fraction of them exhibit strong Fe II multiplets (Boroson & Green 1992). Some NLS1 galaxies show blueshifted line profiles in high-ionisation lines, indicating outflows (e.g., Zamanov et al. 2002; Boroson 2005; Komossa et al. 2008; Berton & Järvelä 2021).

NLS1 galaxies are intrinsically different from broad-line Seyfert (BLS1) galaxies, for example, in their black hole masses, Eddington ratios, and their multi-wavelength and variability properties. The general consensus is that, unlike BLS1 galaxies, NLS1 galaxies are powered by low-mass central supermassive black holes ($M_{\mathrm{BH}} \sim 10^6 \, M_\odot - 10^8 \, M_\odot$; e.g., Peterson 2011; Järvelä et al. 2015; Cracco et al. 2016; Chen et al. 2018). This has been confirmed, for example, by reverberation mapping campaigns (e.g., Wang et al. 2016; Du et al. 2018; Du & Wang 2019). Due to the low black hole mass, NLS1 galaxies are thought to be in an early evolutionary stage with respect to BLS1

galaxies and other classes of AGN (Mathur 2000). They also exhibit high Eddington ratios, generally between 0.1 and 1, but in some cases they also exceed unity (Boroson & Green 1992; Marziani et al. 2018; Tortosa et al. 2022).

NLS1 galaxies have previously been thought to not have significant radio emission (Komossa et al. 2006; Järvelä et al. 2015). Of the currently identified NLS1 galaxies, roughly one-sixth, ~16%, have been detected at radio frequencies: ~6% are weak radio emitters and ~10% have significant radio emission (Komossa et al. 2006). The rest of the NLS1 galaxies, ~84%, have not been detected at radio frequencies yet.

Finding disk galaxies, such as BLS1 galaxies, with jets is not uncommon (Keel et al. 2006; Bagchi et al. 2014; Wu et al. 2022; Gao et al. 2023); however, these sources generally have stellar masses similar to those of elliptical galaxies and are thus atypical among disk-like galaxies. NLS1 galaxies, on the other hand, have pseudo-bulges and low Sérsic indices, indicating that their stellar masses are low (Sánchez Almeida 2020). Thus the discovery of relativistic jets in some NLS1 galaxies was unexpected. These jets appear similar to, but less powerful than, those in blazars (e.g., Komossa et al. 2006; Zhou et al. 2006; Yuan et al. 2008; Foschini 2011; Foschini et al. 2015; Lähteenmäki et al. 2017, 2018). Typically, relativistic jets strongly manifest in the radio frequencies and dominate in the whole band. However, examples of jetted sources with extremely weak low-frequency (<10 GHz) radio emission have also been found (Järvelä 2018; Berton et al. 2020; Järvelä et al. 2021, and in prep.; Sbarrato et al. 2021), bringing into question whether

---

Table 1. Radio properties of the sample (F = flat, S = steep) and the black hole mass estimates.

Source	$S_{1.4\,\mathrm{GHz}}$	$S_{5.5\,\mathrm{GHz}}$	$\log M_{\mathrm{BH}}$		
J0622−2317	4.3	0.9	6.47	F	Diffuse
J0952−0136	59.8	21.3	6.33	S	Jetted
J1511−2119	46.9	18.2	6.63	S	Jetted?
J1522−0644	14.4	5.5	6.66	S	Compact
J1615−0936		0.7	6.94	S	Jetted?
J1628−0304		0.1	6.72	F	Compact
J1646−1124	38.3	10.8	7.07	S	Compact

Notes. All values and radio properties are from Chen et al. (2020). Columns: (1) Source name, (2) 1.4 GHz FIRST maximum flux density level, (3) 5.5 GHz maximum flux density, (4) black hole mass, (5) radio spectrum, and (6) radio morphology

the emission in this regime can be utilised as a proxy for jet-tedness. The opposite has also been observed when sources with significant radio emission at low frequencies do not host relativistic jets, even though that would be expected (Järvelä et al. 2022). This anomaly is caused by the presence of significant star formation activity (Caccianiga et al. 2015; Ganci et al. 2019; Berton et al. 2020).

There have been several individual source analysis studies (Antón et al. 2008; León Tavares et al. 2014; Kotilainen et al. 2016; D'Ammando et al. 2017, 2018; Olguín-Iglesias et al. 2017; Berton et al. 2019; Hamilton et al. 2021; Vietri et al. 2022), as well as numerous large sample studies of the hosts of NLS1 nuclei (Krongold et al. 2001; Crenshaw et al. 2003; Ohta et al. 2007; Orban de Xivry et al. 2011; Mathur et al. 2012; León Tavares et al. 2014; Järvelä et al. 2017; Olguín-Iglesias et al. 2020; Varglund et al. 2022). Nearly all of these studies have identified them as disk-like. Elliptical hosts have been an anomaly; however, some cases seem to exist (D'Ammando et al. 2017, 2018).

For this work we examined the hosts of seven southern NLS1 galaxies that are also part of an optical spectral study and a multi-frequency radio imaging study. This is the first systematic host galaxy investigation of southern NLS1 galaxies, and will be expanded in the future to allow for a statistically significant comparison of their radio and optical properties. Our goal was to determine the morphology of the hosts to improve the statistical weight of the recent findings that most NLS1 nuclei are hosted in disk-like galaxies. Furthermore, we also studied the colour maps as they could tell us more about the properties of the core, such as its dust content, and shed light on a possible merger history. Ultimately, NLS1 galaxies as early-stage AGN, and conveniently residing in the local Universe, can elucidate the evolution of AGN over cosmic time. Throughout this paper we assume a standard λCDM cosmology with parameters $H_0 = 73\,\mathrm{km\,s^{-1}\,Mpc^{-1}}$, $\Omega_{\mathrm{matter}} = 0.27$, and $\Omega_{\mathrm{vacuum}} = 0.73$ (Spergel et al. 2007).

2. Observations and data reduction

Our sample of seven sources was selected from Chen et al. (2018). Our selection criteria were based on the sources' radio properties and the possible presence of jets (Chen et al. 2020). The sources chosen for this study have all been detected at 5.5 GHz, with five of them also having been detected at 1.4 GHz. We present the radio flux densities as well as some basic characteristics of our earlier observations in Table 1. The

radio spectrum of five of the sources is steep, while the final two sources have a flatter spectrum. Based on the results of Chen et al. (2020), J0952−0136, J1511−2119, and J1615−0936 were expected to harbour relativistic jets. J0952−0136 has also been identified as a jetted source by Doi et al. (2015). To investigate the radio properties of the Chen et al. (2020) sample in more detail, we have obtained *Karl G. Jansky* Very Large Array observations in 15, 22, and 33 GHz (Berton et al., in prep.). All of our sources have a low redshift (<0.1) and were observed with FourStar, mounted on the 6.5 m *Magellan* Telescope. Five sources were observed in July 2019, while the rest were observed in February 2020. One source, J0952−0136, was saturated and could not be modelled.

The field of view (FoV) of FourStar is $5.4' \times 5.4'$, with a scale of $0.159''\,\mathrm{px}^{-1}$. All of our sources were observed in both *J* and *Ks* bands. When observing in the *J* band, we used four-point dithering for all sources but J0622−2317 for which we used six-point dithering due to its brightness. In the *Ks* band, the dithering used was six-point for all sources.

For data reduction, we used the Image Reduction and Analysis Facility (IRAF) software. We first created a flat field image for each source for each respective band, to remove eventual signatures in the data produced by the instrument. This flat was applied to each dithered image. After creating the flat field, we combined the dithered images to produce one image per each dithering sequence. Then we continued by creating a superflat to remove the final effects of the background. As a result, the mean sky value is essentially zero. To finalise the reduction, we aligned the created images and combined them. The data reduction process was done for both filters. After producing the final images, we determined the zero point magnitude for each source in both bands using Two Micron All-Sky Survey[1] (2MASS) magnitudes.

3. Data analysis

To perform the photometric decomposition of the host, we used the band with better seeing (see Table 2), which in all cases of this study was the *J* band. *Ks* band images were only used to create the colour maps. Our goal was to determine the host galaxy morphology and the related model parameters that best describe the source.

To perform the photometric decomposition, we followed the same procedure as described in Varglund et al. (2022) with a few exceptions. The point spread function (PSF) model was primarily built with DAOPHOT and secondarily through choosing a star from the image. No separate PSF stars were observed for this project. Furthermore, our cutout image sizes were either $\sim 100 \times 100\,\mathrm{px}$ or $\sim 200 \times 200\,\mathrm{px}$. The size of the image was dependent on the cutout size around the host galaxy we were modelling. The sky background parameter was estimated through two methods: the method described in Varglund et al. (2022) and by using a large annulus that encompassed roughly a fifth of our image. We made sure that no source was inside the annulus before determining the sky background value. The former method was used to confirm the results of the latter method. Due to the used data reduction process, the sky background value was virtually zero.

The fitting process with GALFIT version 3 (Peng et al. 2010), creating the radial surface plot with the IRAF (Stetson 1987) task ELLIPSE, and the error estimation method was identical to the process in Varglund et al. (2022). The radial surface

---

[1] https://www.ipac.caltech.edu/2mass

Table 2. Basic properties of the sample and the observations.

Source	Short name	z	Scale (kpc/″)	RA (J2000.0)	Dec (J2000.0)	Exp (J) (s)	Exp (Ks) (s)	Date (year/month/day)	Seeing (″)
6dFGS J0622335−231742	J0622−2317	0.019	0.370	06:22:34	−23:17:42	960	384	2020/02/08	0.7
6dFGS J0952191−013644	J0952−0136	0.037	0.705	09:52:19	−01:36:44	583	384	2020/02/08	1.0
6dFGS J1511598−211902	J1511−2119	0.044	0.832	15:12:00	−21:19:02	640	384	2019/07/19	0.8
6dFGS J1522287−064441	J1522−0644	0.083	1.500	15:22:29	−06:44:41	640	384	2019/07/20	0.7
6dFGS J1615191−093613	J1615−0936	0.064	1.182	16:15:19	−09:36:13	640	384	2019/07/20	0.7
6dFGS J1628484−030408	J1628−0304	0.092	1.645	16:28:48	−03:04:08	640	384	2019/07/20	0.6
6dFGS J1646104−112404	J1646−1124	0.074	1.351	16:46:14	−11:24:04	872	523	2019/07/20	0.7

Notes. Columns: (1) Source name, (2) short name of the source, (3) redshift, (4) scale at the redshift of the source, (5) right ascension, (6) declination, (7) total exposure time in the J band, (8) total exposure time in the Ks band, (9) observation dates, and (10) average seeing during the observations measured from the images in the band used for modelling.

plot was created to study both the accuracy of the fit as well as to see how the brightness of the components changes as a function of the distance from the core. On average, the limiting surface brightness of the images is around 22–23 mag arcsec^{-2}, whereas all of our sources are considerably brighter than the limit, and thus we can model them reliably up to large radii.

In the case of a suspected bar component based on the best-fit parameters, we used an additional diagnostic to determine if the component truly is a bar. To do this, we extracted the position angle (PA) and ellipticity parameters of the isophotes obtained from the ELLIPSE output of the galaxy image. These parameters were plotted against the radius. The plot indicates the presence of a bar if there is a region in which the ellipticity increases while the PA remains mostly constant (ΔPA $< 20°$; Wozniak et al. 1995; Menéndez-Delmestre et al. 2007).

Finally, since we had images from two bands for each source, we were able to create colour maps of all of our sources. To obtain the colour map, we used the equation below:

$$\text{Colour image pixel value} = (\text{zp}_J - \text{zp}_{Ks}) - 2.5\left[\log_{10}\left(\frac{J}{Ks}\right)\right]. \tag{1}$$

The data used when calculating the colour image were corrected for the different exposure times of the bands. The images were aligned by using GEOMAP, GEOTRAN, and IMALIGN to guarantee that the images were perfectly aligned. The data processing allowed for the PSFs to be nearly identical, improving the colour maps. In the above equation, zp stands for the zero point magnitude, with the subscript defining the band in question. The contour levels in the maps are defined using the Ks band image sky standard deviation (std) and are at 20, 40, 60, 80, 100, 180, 360, 720, and 1440 × std.

4. Individual source analysis

4.1. J0622−2317

According to Chen et al. (2020), this source has a flat in-band radio spectrum, and a diffuse radio morphology. Additional information of this source and all the sources of our sample can be found in Table 1. A visual inspection shows a very clear spiral structure and even hints at the existence of a bar (Fig. 1).

The size of the fitting region was limited due to a nearby, very bright, saturated star. The best-fit results can be seen in Table 3. In addition to the NLS1, three nearby sources were also fitted

using the PSF model to obtain a more realistic χ_ν^2 for the FoV. We have most likely fitted a disk, or a combination of a disk and a pseudo-bulge component that cannot be separated and modelled individually. The bulge may be unresolved, but its light is still present in the image, thus affecting the model, or the bulge is either not bright enough or does not have properties that are different enough compared to the disk. The component is small; however, the Sérsic index is high for a disk, so it is possible that a bulge component is included. The intensity plots of the source can be seen in Fig. 1. There are clear residuals left due to the spiral arms and some slight residuals near the core of the galaxy. We tried to include a bar in the model, but were unable to obtain good results.

The radial surface plot can be seen in Fig. 2. As expected, the model image curve does not follow the curve for the galaxy image perfectly. This is most likely due to the spiral arms not being completely modelled. The colour map can be seen in Fig. 3. On average, Seyfert galaxies have a $J - Ks$ magnitude between 0 and 2.5, and when the magnitude difference is 1.3 or more, a galaxy is considered red (Jarrett 2000). Unlike typical Seyfert galaxies, J0622−2317 is blue. However, the magnitude of the core of the galaxy is above zero, and it is thus within a common range found in NLS1 galaxies. As with the other images, the spiral arms are clearly visible in the colour map.

4.2. J1511−2119

This is one of the three jetted sources in this study. Its radio map can be found in Chen et al. (2020). We used a DAOPHOT PSF model when fitting it. There were ten nearby sources in our FoV, all of which we were able to be fitted with a single PSF with very few residuals.

Our fit models a combination of a disk and a bulge (Table 4). The Sérsic index of 2.96 does not strongly support any specific morphology, even though indices this high can also be found in spiral galaxies (Elmegreen & Elmegreen 2014). The size of the galaxy is typical for an NLS1 host. The excess residuals (Fig. 4) near the core imply the presence of unmodelled structures, such as leftover fragments of the bulge. The galaxy, model, and Sérsic curves in the radial surface brightness plot, Fig. 5, are all very similar to each other.

The host galaxy of J1511−2119 is disk-like, and based on the Sérsic index, an S0 galaxy. The colour map, shown in Fig. 6, shows colours commonly seen in NLS1 galaxies, with the red most likely signifying dust extinction. The core of the galaxy is extremely red as the $J - Ks$ magnitude is ∼2. Beyond the core, the galaxy has very uniform colours.
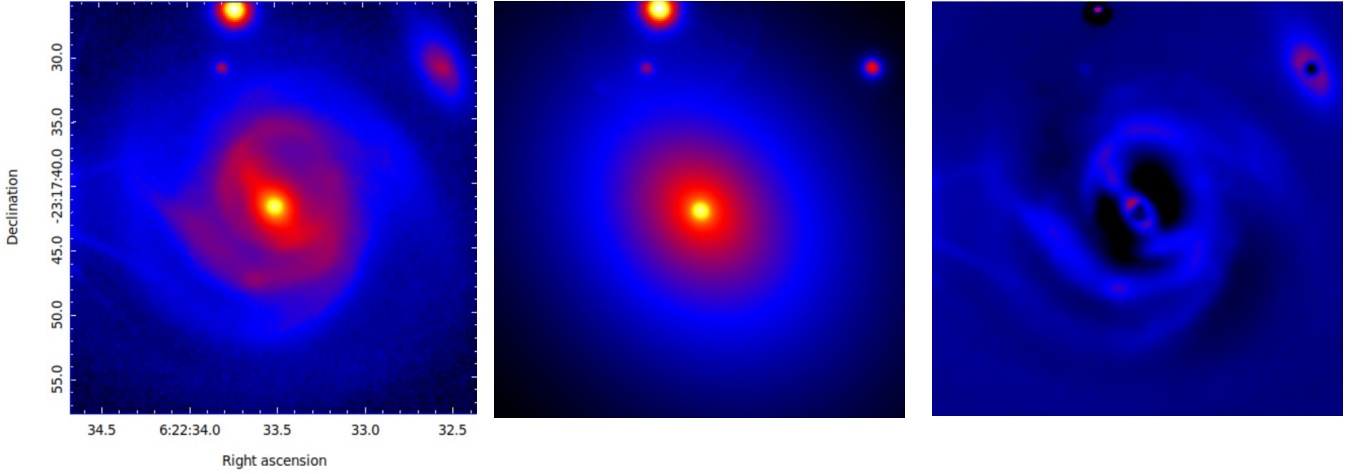
Fig. 1. *J* band images of J0622−2317. The FoV is 31.8″/11.8 kpc in all images. *Left panel*: observed image. *Middle panel*: model image. *Right panel*: residual image, smoothed over 3 px.

Table 3. Best-fit parameters of J0622−2317.

Function	Mag	r_e (kpc)	n	Axial ratio	PA (°)	Notes
PSF 1	$14.70^{+0.01}_{-0.01}$					
Sérsic 1	$11.98^{+0.01}_{-0.02}$	$3.20^{+0.19}_{-0.00}$	$1.65^{+0.01}_{-0.00}$	$0.80^{+0.00}_{-0.00}$	$41.91^{+0.01}_{-0.02}$	Disk and bulge

Notes. We note that $\chi^2_\nu = 0.988^{+0.00}_{-0.00}$. Columns: (1) Function used for modelling, (2) magnitude, (3) effective radius, (4) Sérsic index, (5) axial ratio, (6) position angle, and (7) additional notes on the sources.
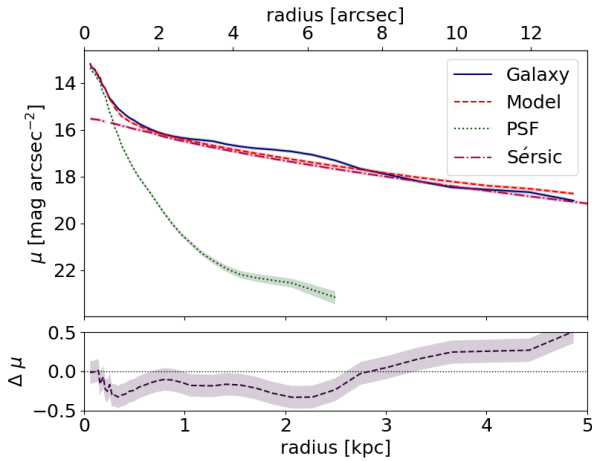
Fig. 2. Radial surface brightness profile plot of J0622−2317. The blue line represents the galaxy component, the dashed red line shows the model, the dotted green line marks the PSF, and finally the dashed pink line shows the Sérsic component. The error of each component is shown by the shaded area surrounding each curve.

4.3. J1522−0644

We successfully used the PSF model to fit the five nearby sources. The source, model, and residual images can be seen in Fig. 7. The best-fit parameters are given in Table 5. Along with a PSF, we used two Sérsic functions for fitting this source. Based on the effective radius of Sérsic 1, it is presumably fitting a disk. The Sérsic index is low for a disk, but not unreasonable. Based on its parameters, the second Sérsic function most likely models a bar. To further study this possibility, we plotted the PA
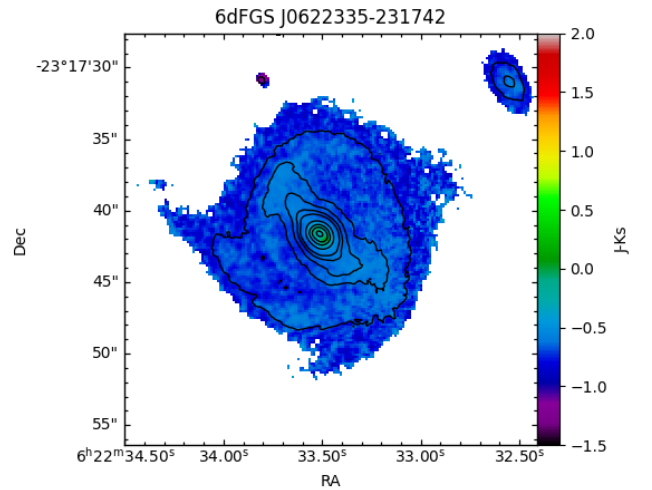
**Fig. 3.** *J* − *Ks* colour map of J0622−2317.

and ellipticity over the radius, seen in Fig. 8. The PA remains steady throughout the plot. The ellipticity increases towards the higher radii. Based on this plot, it is difficult to confirm whether or not Sérsic 2 truly models a bar. The remaining residuals of the source are mostly remnants of the spiral arms.

The χ^2_ν is relatively high due to the remaining residuals, but the fit is satisfactory and the radial surface plot, Fig. 9, supports the goodness of the fit. The galaxy and the model curves match. The colour magnitude, seen in Fig. 10, of the galaxy is as expected in an NLS1 galaxy. The $J − Ks$ magnitude near the core is approximately 1.75, and is thus very red. The redness of the core is most likely due to dust extinction.

Table 4. Best-fit parameters of J1511−2119.

Function	Mag	r_e (kpc)	n	Axial ratio	PA (°)	Notes
PSF 1	$14.24^{+0.03}_{-0.03}$					
Sérsic	$15.90^{+0.03}_{-0.03}$	$3.93^{+0.15}_{-0.00}$	$2.96^{+0.08}_{-0.00}$	$0.90^{+0.00}_{-0.00}$	$-70.82^{+0.00}_{-0.12}$	Bulge and disk

Notes. We note that $\chi^2_\nu = 0.916^{+0.00}_{-0.02}$. Columns: (1) Function used for modelling, (2) magnitude, (3) effective radius, (4) Sérsic index, (5) axial ratio, (6) position angle, and (7) additional notes on the sources.
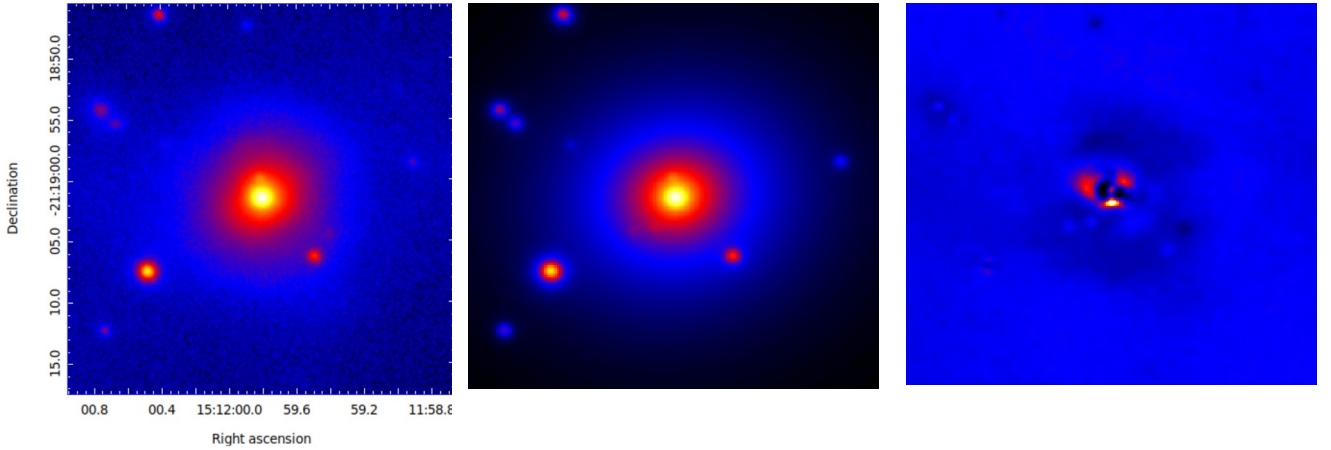
Fig. 4. J band images of J1511−2119. The FoV is 31.8″/26.5 kpc in all images. *Left panel*: observed image. *Middle panel*: model image. *Right panel*: residual image, smoothed over 3 px.
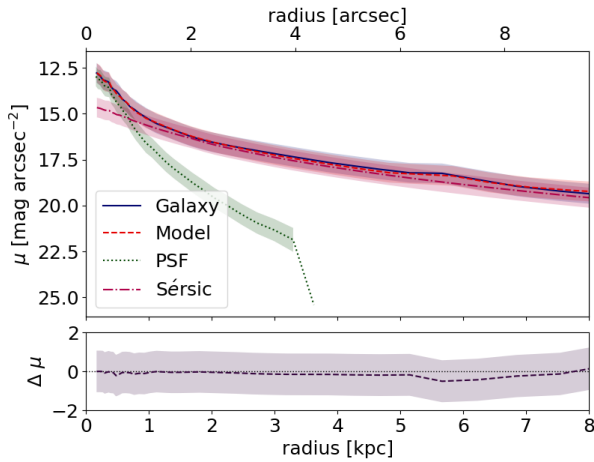
Fig. 5. Radial surface brightness profile plot of J1511−2119. The blue line represents the galaxy component, the dashed red line shows the model, the dotted green line marks the PSF, the dashed pink line shows the Sérsic 1 component, and the final component, Sérsic 2, is shown with the dotted light blue line. The error of each component is shown by the shaded area surrounding each curve.

4.4. J1615−0936

We tried to model the PSF with DAOPHOT and by directly using a nearby star. Based on our results, the DAOPHOT PSF provided a better model. The unsatisfactory fit of the nearby source increases the χ^2_ν of the fit.

We modelled the source with a PSF, a Sérsic function, and an exponential disk function. The best-fit parameters can be found in Table 6. Despite several attempts and different approaches, the χ^2_ν remained quite high. Based on our best-fit results, the Sérsic
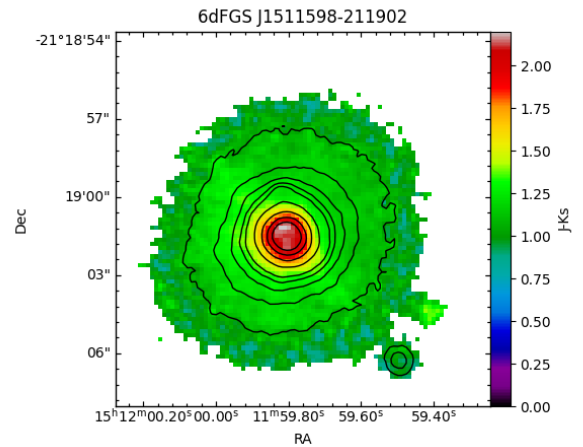
Fig. 6. $J - Ks$ colour map of J1511−2119.

represents a pseudo-bulge and the exponential disk function naturally fits a disk. There are some clear residuals left, as seen in Fig. 11. The residuals of the NLS1 are most likely caused by the bright AGN that was hard to model due to the lack of a bright enough PSF star.

The χ^2_ν of the fit is not ideal; however, it does not always imply that the fit is physically unreasonable (Dewsnap et al. 2023). Indeed, based on the radial surface brightness plot, seen in Fig. 12, our model is accurate, as there is virtually no deviation between the model and galaxy curves, and the obtained components are physically reasonable. Based on our results, the host galaxy of J1615−0936 is disk-like, resembling a lenticular galaxy. This is supported by the axial ratio of the disk component being so small, $0.29^{+0.00}_{-0.00}$.
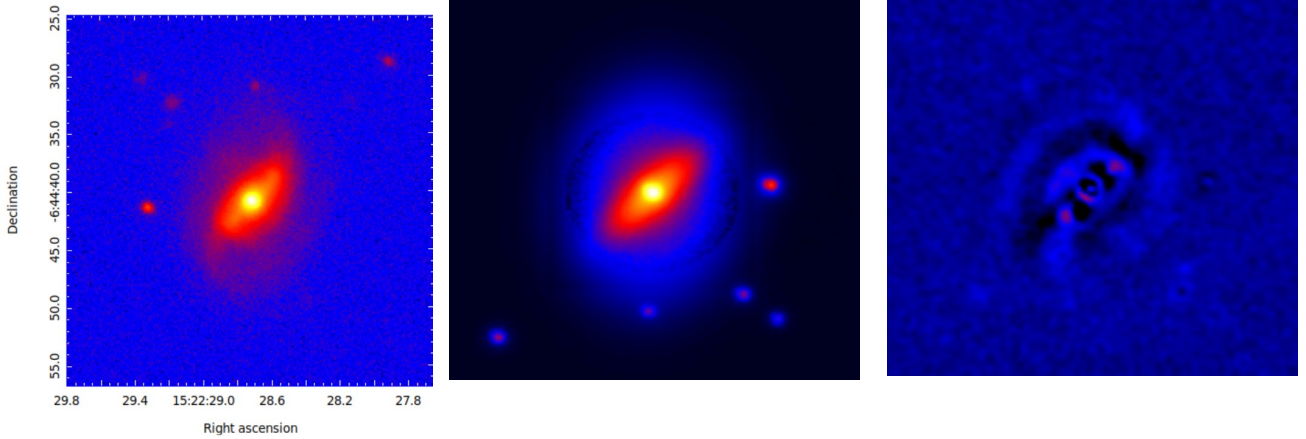
Fig. 7. *J* band images of J1522−0644. The FoV is 31.8″/47.7 kpc in all images. *Left panel*: observed image. *Middle panel*: model image. *Right panel*: residual image, smoothed over 3 px.

Table 5. Best-fit parameters of J1522−0644.

Function	Mag	r_e (kpc)	n	Axial ratio	PA (°)	Notes
PSF 1	$15.55^{+0.05}_{-0.05}$					
Sérsic 1	$14.76^{+0.01}_{-0.00}$	$7.72^{+0.02}_{-0.02}$	$0.48^{+0.01}_{-0.01}$	$0.76^{+0.00}_{-0.00}$	$-5.97^{+0.02}_{-0.02}$	Disk
Sérsic 2	$15.19^{+0.00}_{-0.00}$	$3.80^{+0.00}_{-0.00}$	$0.61^{+0.00}_{-0.00}$	$0.36^{+0.00}_{-0.00}$	$-44.74^{+0.01}_{-0.01}$	Bar

Notes. We note that $\chi^2_\nu = 1.257^{+0.03}_{-0.03}$. Columns: (1) Function used for modelling, (2) magnitude, (3) effective radius, (4) Sérsic index, (5) axial ratio, (6) position angle, and (7) additional notes on the sources.
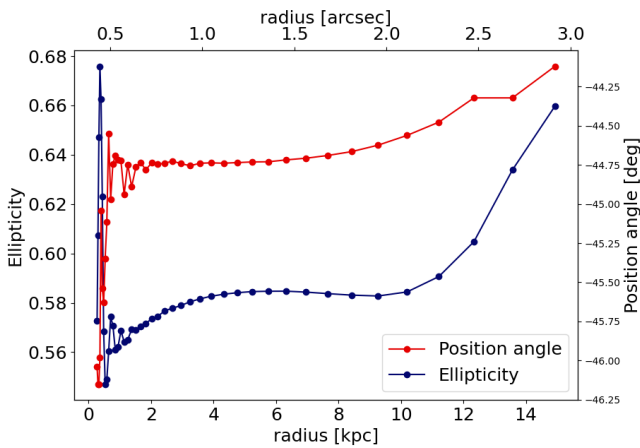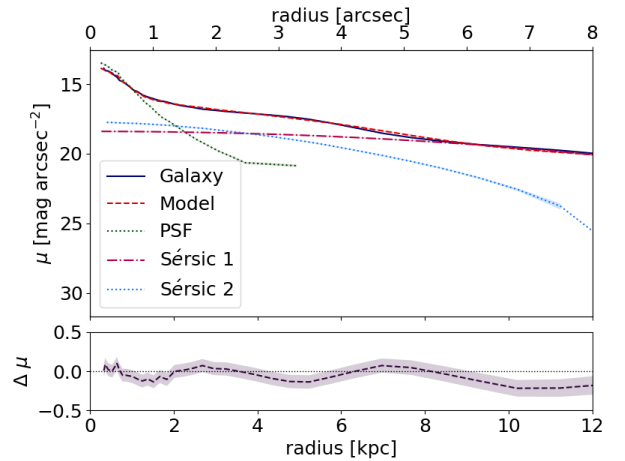

Fig. 8. Position angle and ellipticity of the Sérsic 1 function plotted against the major axis of the isophote of J1522−0644.

Fig. 9. Radial surface brightness profile plot of J1522−0644. The blue line represents the galaxy component, the dashed red line shows the model, the dotted green line marks the PSF, and finally the dashed pink line shows the Sérsic component. The error of each component is shown by the shaded area surrounding each curve.

The colour map of J1615−0936 is presented in Fig. 13. Based on it, the core has a $J - Ks$ colour magnitude of roughly 1.5, which means that the core of the galaxy is very red. The rest of the galaxy presents uniform colours. Overall, the colours of the galaxy are as would be expected in an NLS1 galaxy.

4.5. J1628−0304

We used a Sérsic function, an exponential disk function, and a PSF to fit the galaxy. The best-fit parameters are shown in Table 7. DAOPHOT provided the best PSF model, but it is not perfect, as evidenced by the remaining residuals seen in Fig. 14

near the core of the galaxy. The Sérsic function models a bar component. The galaxy is small, also proven by the small effective radius of the exponential disk component. We plotted the ellipticity and PA against the radius of the isophotes, seen in Fig. 15, to study the possible bar. In the plot the ellipticity can be seen to increase while the PA is more or less constant. The plot strongly suggests that the Sérsic function does indeed model a bar component.

The χ^2_ν for this source is quite high. However, there are virtually no high surface brightness residuals left. The remaining
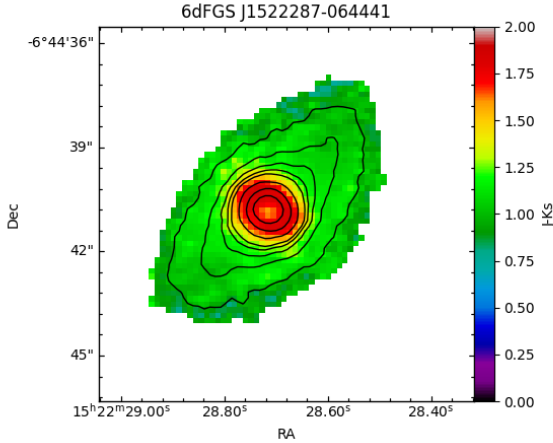
Fig. 10. $J - Ks$ colour map of J1522−0644.

residuals are likely caused by the imperfect PSF model, which we could not improve despite several attempts with different methods. A major issue with the PSF modelling was the lack of bright enough stars in the FoV – none of them are brighter than the AGN, and probably cannot model the wings of the PSF accurately. However, as discussed earlier, the χ^2_ν value does not alone determine if the fit is physically justifiable and we want to emphasise the importance of also taking into account the obtained components, the residuals, and the comparison between the galaxy and the model, in Fig. 16, when evaluating the fit. Based on all of these aspects, the obtained results are adequate. The host galaxy of J1628−0304 is disk-like.

The colour map can be seen in Fig. 17. The colours of this galaxy interest as the reddest part is not at the core, but rather surrounds it. The structure could be due to a star-forming ring or a minor merger (Iodice et al. 2014). However, the resolution of our images does not allow for a detailed view of the possible minor merger and, due to this, the feature is most likely a star-forming ring. Circumnuclear star-forming rings have been frequently observed in NLS1 galaxies (Winkel et al. 2022). Nonetheless, the core has a colour magnitude of ~1.5 and is thus very red.

4.6. J1646−1124

This source has a high χ^2_ν value (Table 8). Despite this, when studying the residuals, seen in Fig. 18, and the best-fit parameters, the fit is acceptable. A PSF was fitted on the five nearby sources as well as on the galaxy. In addition, the galaxy required one Sérsic function, with the function most likely modelling a bulge. The Sérsic index is high for a spiral galaxy, though still within the range of accepted values for them. We attempted to fit additional components, but could not achieve a physically justifiable fit. Our issues mostly stem from the AGN being so bright. A fit with three Sérsic functions yielded a better χ^2_ν (2), but one of the components consistently remained unresolved, likely trying to fit parts of the point-like AGN. The resolved components modelled a bulge and a disk component. The alternative-fit results can be seen in Table 9.

Some residuals still remain near the galaxy core, and are most likely due to the issues with the PSF model. There is an indication of a spiral-like structure surrounding the galaxy, starting from its west side, and bending anti-clockwise towards the east. However, without further proof, the assessment of the residuals remains a speculation. Due to the χ^2_ν value, the residuals, and the best-fit parameters, we do not deem it possible to irrefutably

determine the host galaxy of J1646−1124. However, there is evidence, for example, in the alternative fit that J1646−1124 is disk-like and, based on the parameters, an S0.

The radial surface plot, seen in Fig. 19, shows that despite the difficulties in the modelling, the model fits the galaxy very well up to the radius of 6 kpc. The colour map of the source can be seen in Fig. 20. The colours are as expected for an NLS1 galaxy, with the core being very red (~2.2). The redness is most likely due to dust extinction. Some slight saturation, resulting in the polygonal shape, due to the Ks image can be seen in the colour map.

5. Discussion

We were able to model six out of the seven sources in our sample. The only source we could not model was J0952−0136. A summary with the final verdicts of each source can be found in Table 10. Two of our modelled sources, J1511−2119 and J1615−0936, have been speculated by Chen et al. (2020) to be jetted based on their radio spectra. All six of our sources have disk-like hosts. The only uncertain host morphology is for J1646−1124; however, our results still suggest the possibility of a disk-like morphology. Three of our sources show evidence for being in lenticular galaxies. However, it is unclear if the morphology is truly lenticular or if the results are caused by the AGN being too bright to have a reliable PSF model from the FoV. We were able to model a disk component in five of our sources, which naturally indicates a disk-like morphology of the galaxy. A bar component can be found in two sources, J1522−0644 and J1628−0304. Based on the PA and ellipticity versus the major axis of the isophote plots, J1628−0304 is very likely to host a bar. We were able to model a bulge component in four sources. The modelled bulges have a slightly high Sérsic index for them to be considered pseudo-bulges in disk-like galaxies. The commonly used limit for distinguishing between pseudo- and classical bulges is $n = 2$, where indices below two are associated with pseudo-bulges and indices above with classical bulges (Orban de Xivry et al. 2011). However, the sources that have bulges with Sérsic indices above two are the sources we suspect of being S0s and it has been suggested that S0/a sources can have pseudo-bulges with a Sérsic index ≈ 2.4 with a standard deviation of 0.66 (Kormendy & Kennicutt 2004). With this in mind, the modelled bulges are most likely pseudo-bulges, which is in agreement with what is seen in disk-like galaxies.

Our findings are in alignment with the majority of previous studies regarding the host galaxy morphology of jetted and non-jetted NLS1 galaxies (e.g., Crenshaw et al. 2003; Ohta et al. 2007; Antón et al. 2008; Orban de Xivry et al. 2011; León Tavares et al. 2014; Kotilainen et al. 2016; Olguín-Iglesias et al. 2017, 2020; Järvelä et al. 2018; Berton et al. 2019; Hamilton et al. 2021; Vietri et al. 2022; Varglund et al. 2022). Only two jetted NLS1 galaxies have thus far been identified to be located in elliptical galaxies (D'Ammando et al. 2017, 2018). However, the morphology of FBQS J1644+2619 being elliptical is up for debate as the source has also been suggested to reside in a barred lenticular galaxy.

Only a few studies on NLS1 galaxy stellar masses exist, and we were able to find a stellar mass estimate for three of our sources: J0952−0136 ($M_{\mathrm{star}} \sim 1.5 \times 10^9\,M_\odot$; Pan et al. 2021), J0622−2317 ($M_{\mathrm{star}} \sim 1.3 \times 10^{10}\,M_\odot$; Saulder et al. 2016), and J1511−2119 ($M_{\mathrm{star}} \sim 1.3 \times 10^{11}\,M_\odot$; Koss et al. 2021). Two of these sources have a low stellar mass, while J1511−2119 has a high stellar mass. The high stellar mass is not surprising as the galaxy is most likely an S0. The stellar mass of J0952−0136

Table 6. Best-fit parameters of J1615−0936.

| Function	Mag	r_e (kpc)	n	Axial ratio	PA (°)	Notes
PSF 1	$14.25^{+0.03}_{-0.03}$					
Sérsic	$14.68^{+0.03}_{-0.03}$	$1.61^{+0.05}_{-0.04}$	$2.74^{+0.15}_{-0.12}$	$0.72^{+0.00}_{-0.00}$	$81.49^{+0.07}_{-0.05}$	Bulge
Exp. disk	$17.62^{+0.03}_{-0.03}$	$2.44^{+0.00}_{-0.03}$		$0.29^{+0.00}_{-0.00}$	$87.69^{+0.00}_{-0.00}$	Disk

Notes. We note that $\chi^2_\nu = 2.553^{+0.02}_{-0.01}$. Columns: (1) Function used for modelling, (2) magnitude, (3) effective radius, (4) Sérsic index, (5) axial ratio, (6) position angle, and (7) additional notes on the sources.
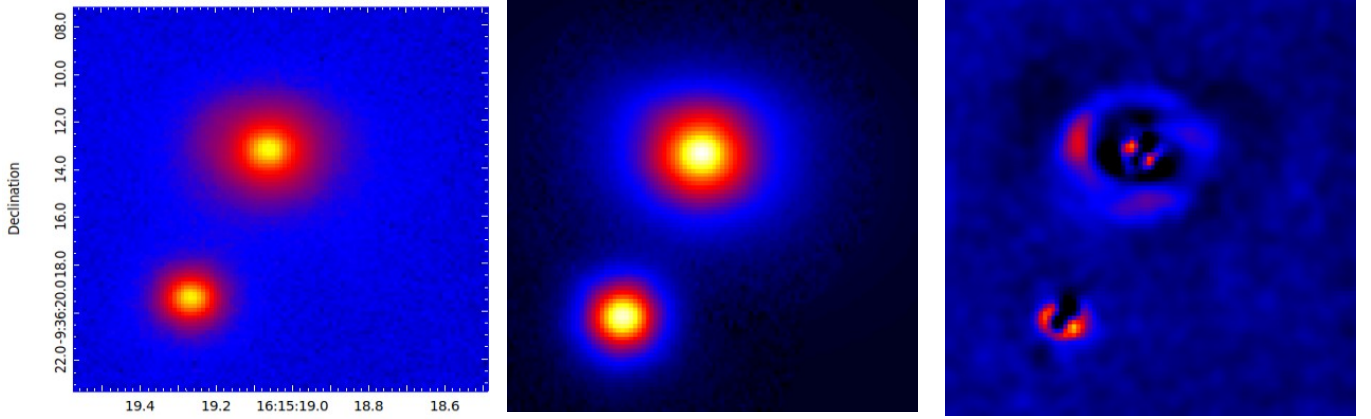
Fig. 11. *J* band images of J1615−0936. The FoV is 15.9″/18.8 kpc in all images. *Left panel*: observed image. *Middle panel*: model image. *Right panel*: residual image, smoothed over 3 px.
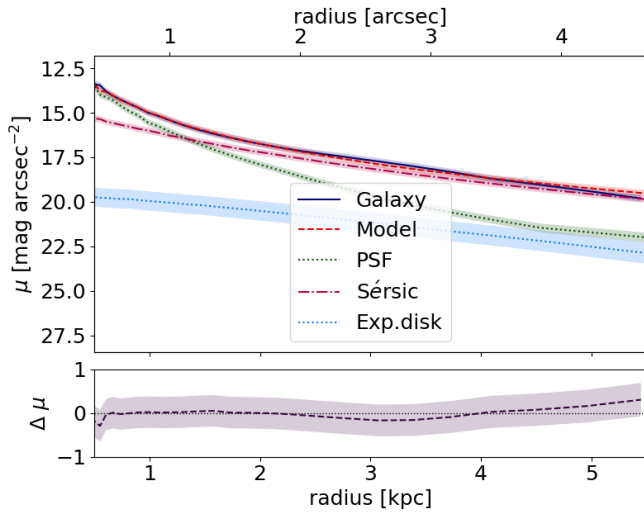
Fig. 12. Radial surface brightness profile plot of J1615−0936. The blue line represents the galaxy component, the dashed red line shows the model, the dotted green line marks the PSF, the dashed pink line shows the Sérsic component, and the final component, the exponential disk, is shown with the dotted light blue line. The error of each component is shown by the shaded area surrounding each curve.
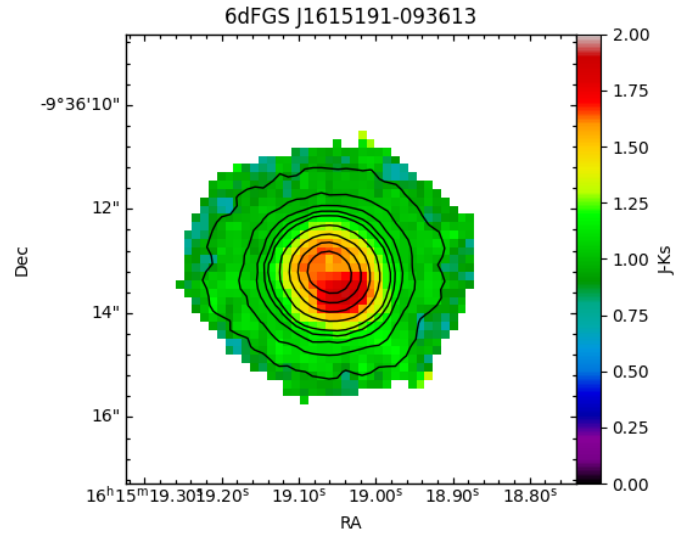
Fig. 13. $J − Ks$ colour map of J1615−0936.

being low is interesting as it is a jetted source; however, as we do not have information of the stellar mass of other jetted NLS1 galaxies, no further conclusions can be drawn. Based on the relation of the stellar mass, and the effective radius and Sérsic index of the NLS1 galaxies of this paper, the stellar mass of these sources is most likely low (Sánchez Almeida 2020).

When studying the evolution of AGN, the nearby environment, both group- and galaxy-scale, is a crucial factor to take into account. This is due to the nearby environment being capable of reshaping the galaxy as well as the galaxy dynamics. It has been hypothesised that jetted NLS1 galaxies are linked to interaction and/or mergers (e.g., Järvelä et al. 2017; Olguín-Iglesias et al. 2020; Berton et al. 2021). However, there is no clear consensus on the topic yet. None of the sources in this paper present clear mergers or an interaction. This could be for a variety of reasons, with one of the possible reasons being the lack of resolution for seeing minor mergers. It has been shown before
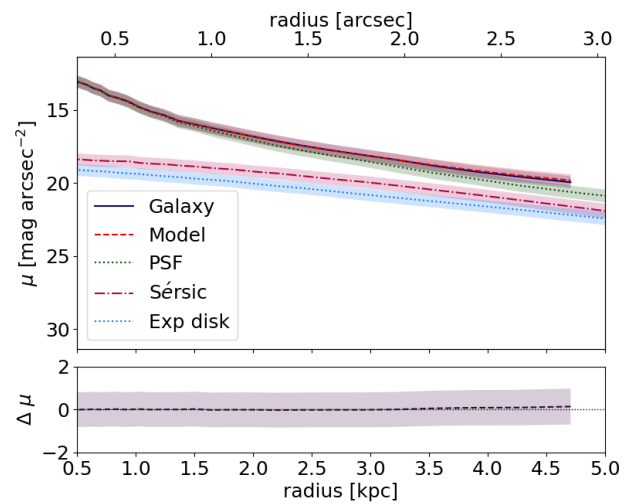
Table 7. Best-fit parameters of J1628−0304.

Function	Mag	r_e (kpc)	n	Axial ratio	PA (°)	Notes
PSF 1	$14.37^{+0.16}_{-0.17}$					
Sérsic	$18.16^{+0.18}_{-0.17}$	$1.92^{+0.03}_{-0.00}$	$0.75^{+0.00}_{-0.00}$	$0.44^{+0.00}_{-0.00}$	$46.06^{+0.15}_{-0.00}$	Bar
Exp. disk	$17.45^{+0.16}_{-0.17}$	$2.00^{+0.01}_{-0.02}$		$0.57^{+0.01}_{-0.00}$	$43.23^{+0.31}_{-0.00}$	Disk

Notes. We note that $\chi^2_\nu = 3.183^{+0.05}_{-0.05}$. Columns: (1) Function used for modelling, (2) magnitude, (3) effective radius, (4) Sérsic index, (5) axial ratio, (6) position angle, and (7) additional notes on the sources.
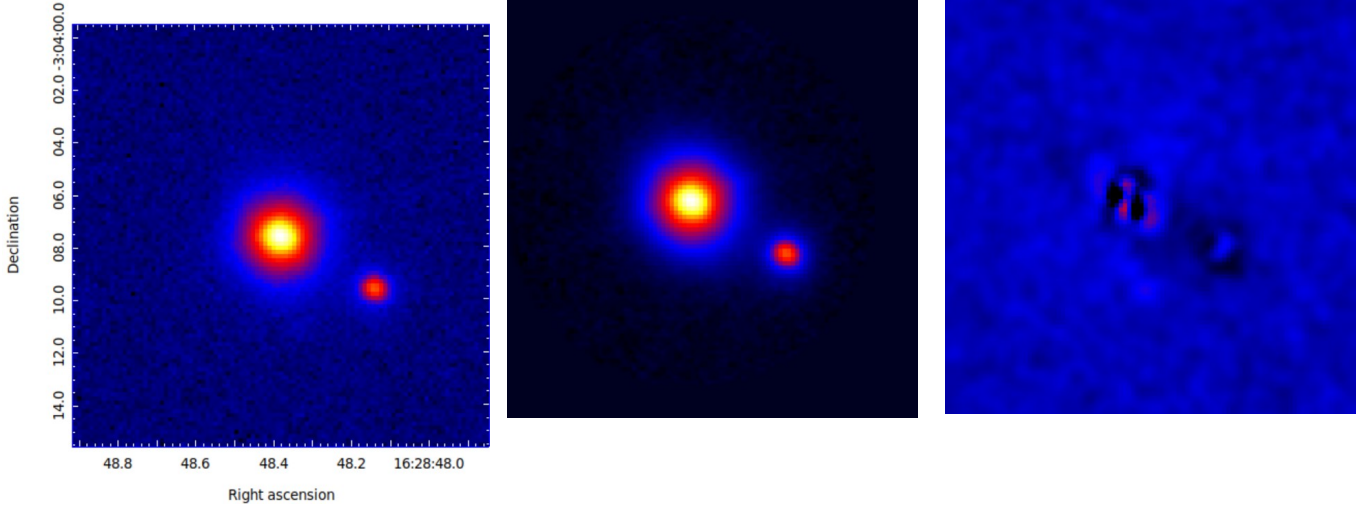
Fig. 14. J band images of J1628−0304. The FoV is 15.9″/26.2 kpc in all images. *Left panel*: observed image. *Middle panel*: model image. *Right panel*: residual image, smoothed over 3 px.
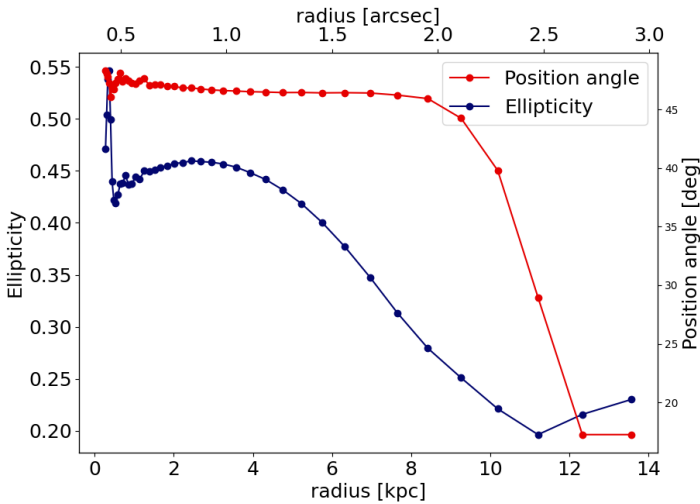
Fig. 15. Position angle and ellipticity of the Sérsic function plotted against the major axis of the isophote of J1628−0304.

Fig. 16. Radial surface brightness profile plot of J1628−0304. The blue line represents the galaxy component, the dashed red line shows the model, the dotted green line marks the PSF, the dashed pink line shows the Sérsic component, and the final component, the exponential disk component, is shown with the dotted light blue line. The error of each component is shown by the shaded area surrounding each curve.

that minor mergers are capable of triggering nuclear activity, an example of this is IRAS 17020+4544. Although this source is a jetted NLS1 galaxy, there is no clear evidence of mergers in optical/near-infrared (NIR) imaging, but there is clear evidence of a small companion galaxy based on molecular gas observations (Salomé et al. 2021; Järvelä et al. 2022).

It has also been speculated that γ-ray-emitting NLS1 galaxies have experienced more minor mergers than non-γ-NLS1

galaxies with significant radio emission (Olguín-Iglesias et al. 2020). The same study also stated that the γ-NLS1 galaxies have bulge colours that are significantly different from their hosts with a red NIR colour, $J - K \sim 2$, while the non-γ-ray NLS1 galaxies have bulge colours that are similar to the rest of the galaxy. The

Table 8. Best-fit parameters of J1646−1124.

Function	Mag	r_e (kpc)	n	Axial ratio	PA (°)	Notes
PSF 1	$13.76^{+0.00}_{-0.00}$					
Sérsic	$14.63^{+0.05}_{-0.06}$	$1.65^{+0.03}_{-0.03}$	$2.68^{+0.15}_{-0.12}$	$0.81^{+0.00}_{-0.00}$	$-72.19^{+0.03}_{-0.05}$	Bulge

Notes. We note that $\chi^2_\nu = 3.221^{+0.02}_{-0.01}$. Columns: (1) Function used for modelling, (2) magnitude, (3) effective radius, (4) Sérsic index, (5) axial ratio, (6) position angle, and (7) additional notes on the sources.

Table 9. Alternative-fit parameters of J1646−1124.

Function	Mag	r_e (kpc)	n	Axial ratio	PA (°)	Notes
PSF 1	$13.83^{+0.00}_{-0.00}$					
Sérsic 1	$15.94^{+0.05}_{-0.06}$	$1.88^{+0.02}_{-0.04}$	$1.38^{+0.04}_{-0.21}$	$0.72^{+0.00}_{-0.00}$	$66.76^{+0.03}_{-0.05}$	Disk
Sérsic 2	$15.78^{+0.04}_{-0.03}$	$0.37^{+0.02}_{-0.03}$	$0.34^{+0.04}_{-0.02}$	$0.17^{+0.00}_{-0.00}$	$13.43^{+0.08}_{-0.05}$	
Sérsic 3	$15.23^{+0.05}_{-0.06}$	$3.11^{+0.24}_{-0.13}$	$2.52^{+0.11}_{-0.12}$	$0.70^{+0.00}_{-0.00}$	$-89.6^{+0.01}_{-0.05}$	Bulge

Notes. We note that $\chi^2_\nu = 2.229^{+0.03}_{-0.04}$. Columns: (1) Function used for modelling, (2) magnitude, (3) effective radius, (4) Sérsic index, (5) axial ratio, (6) position angle, and (7) additional notes on the sources.
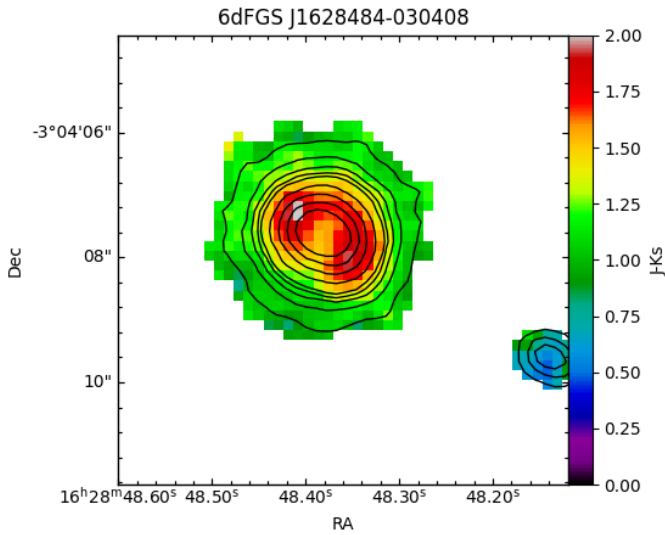
Fig. 17. $J - Ks$ colour map of J1628−0304.

red nuclei are, according to the authors, most likely due to either the bulge showing enhanced star formation or the AGN being dust-embedded as a consequence of a past minor merger. Contradictory to the results in Olguín-Iglesias et al. (2020), all but one of the sources in this paper showcase the nucleus being significantly redder than the rest of the galaxy. The only exception to this is J0622−2317; however, it is possible that the colouration difference in this source is due to the spiral arms beginning directly from the core, and thus 'hiding' the core under the spiral arms. In case the speculation by Olguín-Iglesias et al. (2020) is indeed correct, it is entirely possible that the colour of the core could also be a hint of previous minor mergers in our sources. However, unlike in Olguín-Iglesias et al. (2020), the nuclei of our sources do not present any clear difference in colours between jetted and non-jetted NLS1 galaxies. Based on the current understanding, it is impossible to say whether or not mergers are needed for triggering powerful relativistic jets in NLS1 galaxies.

6. Conclusions

We have studied six NLS1 galaxies that have been observed in J and Ks bands. The observations were carried out with the FourStar NIR instrument. The goal of our study was to investigate what morphology the host galaxies of our sources have. We also created colour maps for all of our sources. These maps were created to help study the properties of the core of the source. Furthermore, we also wanted to study a possible interaction in our sources. The main findings of our study are as follows:

1. All of our sources are most likely located in disk-like galaxies, including the possibly jetted NLS1 galaxies.
2. The colour maps show that the core of NLS1 galaxies strongly tends towards the red side, with no significant difference between the cores of jetted and non-jetted NLS1 galaxies.
3. The redness of the core is most likely due to either dust extinction or due to previous minor mergers.

With over 100 studied hosts of NLS1 galaxies, jetted and non-jetted, the host galaxies of all types of NLS1 nuclei can be stated to be predominantly disk-like. What is still mostly missing is the information regarding the host galaxies of NLS1 sources at high redshifts, and more observations will be needed to determine if their properties are similar to their low-redshift counterparts. Suitable instruments for these studies would be, for example, the Very Large Telescope as well as the JWST. Multi-wavelength observations are crucial for understanding the role of mergers and an interaction in jetted NLS1 galaxies. For this, observations with the Atacama Large Millimeter Array at sub-millimetre wavelengths would be a key factor. NLS1 galaxies offer a unique opportunity to study the interplay of different phenomena, such as jets, outflows, and star formation, at an early stage of AGN evolution, and to estimate the impact an active nucleus has on the galaxy evolution.
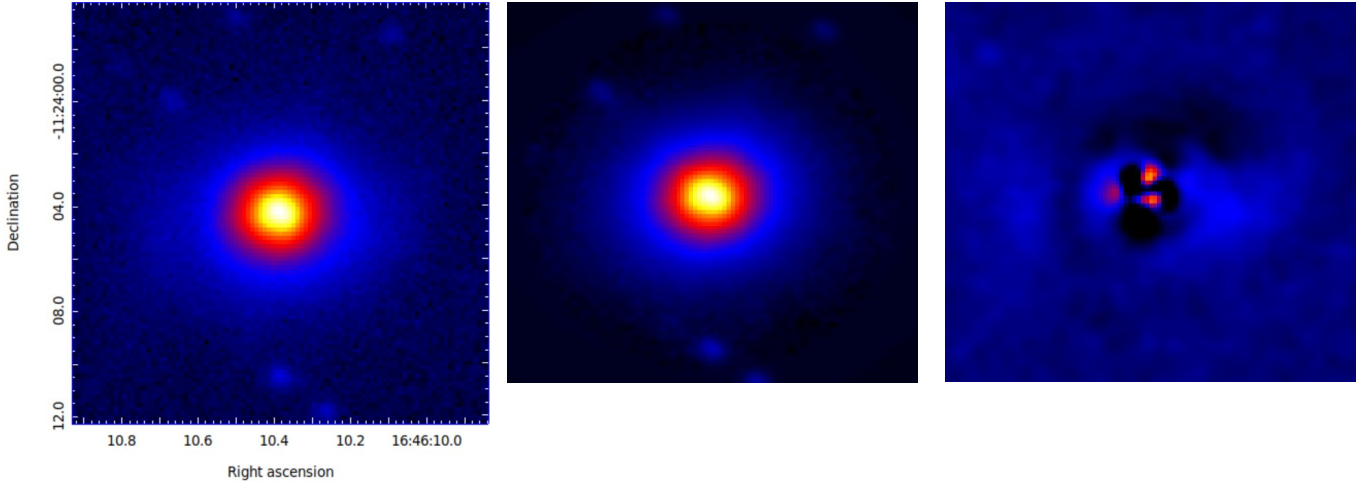
Fig. 18. *J* band images of J1646−1124. The FoV is 15.9″/21.5 kpc in all images. *Left panel*: observed image. *Middle panel*: model image. *Right panel*: residual image, smoothed over 3 px.

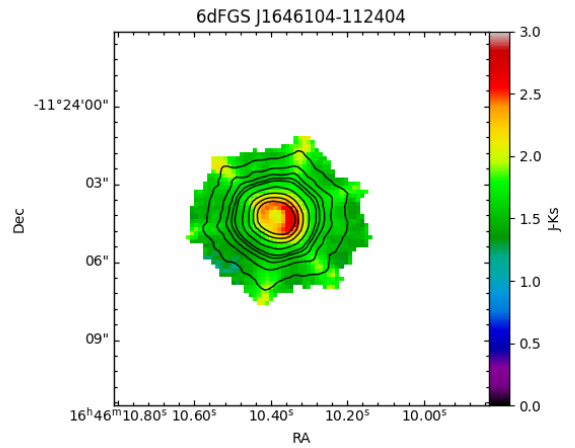**Table 10.** Summary of the results.

Source	Morphology	Components	Jetted	Notes
6dFGS J0622335−231742	Disk-like	Disk and bulge	No	
6dFGS J0952191−013644	Unclear		Yes	Saturated image
6dFGS J1511598−211902	Disk-like	Disk and bulge	Yes	Possibly S0
6dFGS J1522287−064441	Disk-like	Disk and bar	No	
6dFGS J1615191−093613	Disk-like	Disk and bulge	Yes	Possibly S0
6dFGS J1628484−030408	Disk-like	Disk and bar	No	
6dFGS J1646104−112404	Disk-like	Bulge	No	Slightly saturated colour map, possibly S0

Notes. Columns: (1) Source name, (2) probable morphology of the host galaxy, (3) components of the model, (4) presence of a relativistic jet based on the Metsähovi 37 GHz detections, (5) large-scale environment parameter, and (6) additional notes.
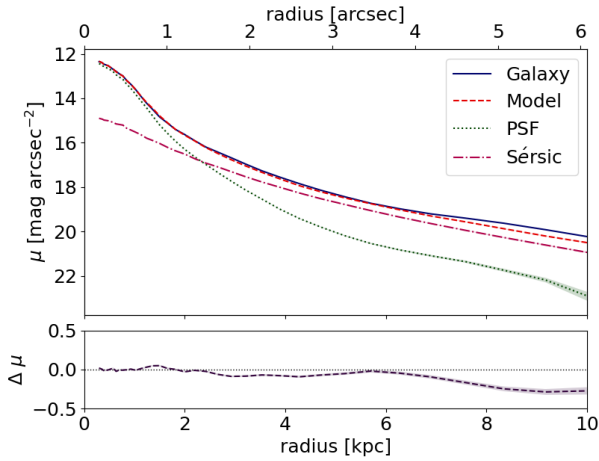
Fig. 19. Radial surface brightness profile plot of J1646−1124. The blue line represents the galaxy component, the dashed red line shows the model, the dotted green line marks the PSF, the dashed pink line shows the Sérsic 1 component, and the final component, Sérsic 2, is shown with the dotted light blue line. The error of each component is shown by the shaded area surrounding each curve.

Fig. 20. $J - Ks$ colour map of J1646−1124.

References

Antón, S., Browne, I. W. A., & Marchã, M. J. 2008, A&A, 490, 583
Astropy Collaboration (Robitaille, T. P., et al.) 2013, A&A, 558, A33
Astropy Collaboration (Price-Whelan, A. M., et al.) 2018, AJ, 156, 123
Bagchi, J., Vivek, M., Vikram, V., et al. 2014, ApJ, 788, 174
Berton, M., & Järvelä, E. 2021, Universe, 7, 188
Berton, M., Congiu, E., Ciroi, S., et al. 2019, AJ, 157, 48
Berton, M., Järvelä, E., Crepaldi, L., et al. 2020, A&A, 636, A64
Berton, M., Peluso, G., Marziani, P., et al. 2021, A&A, 654, A125
Boroson, T. 2005, AJ, 130, 381
Boroson, T. A., & Green, R. F. 1992, ApJ, 80, 109
Caccianiga, A., Antón, S., Ballo, L., et al. 2015, MNRAS, 451, 1795
Chen, S., Berton, M., La Mura, G., et al. 2018, A&A, 615, A167
Chen, S., Järvelä, E., Crepaldi, L., et al. 2020, MNRAS, 498, 1278
Cracco, V., Ciroi, S., Berton, M., et al. 2016, MNRAS, 462, 1256
Crenshaw, D. M., Kraemer, S. B., & Gabel, J. R. 2003, AJ, 126, 1690
D'Ammando, F., Acosta-Pulido, J. A., Capetti, A., et al. 2017, MNRAS, 469, L11
D'Ammando, F., Acosta-Pulido, J. A., Capetti, A., et al. 2018, MNRAS, 478, L66
Dewsnap, C., Barmby, P., Gallagher, S. C., et al. 2023, ApJ, 944, 137
Doi, A., Wajima, K., Hagiwara, Y., & Inoue, M. 2015, ApJ, 798, L30
Du, P., & Wang, J.-M. 2019, ApJ, 886, 42
Du, P., Brotherton, M. S., Wang, K., et al. 2018, ApJ, 869, 142
Elmegreen, D. M., & Elmegreen, B. G. 2014, ApJ, 781, 11
Foschini, L. 2011, in Narrow-Line Seyfert 1 Galaxies and their Place in the Universe, eds. L. Foschini, M. Colpi, L. Gallo, et al., 24
Foschini, L., Berton, M., Caccianiga, A., et al. 2015, A&A, 575, A13
Ganci, V., Marziani, P., D'Onofrio, M., et al. 2019, A&A, 630, A110
Gao, X. Y., Yuan, Z. S., Han, J. L., Wen, Z. L., & Shan, S. S. 2023, RAA, 23, 035005
Goodrich, R. W. 1989, ApJ, 342, 224
Hamilton, T. S., Berton, M., Antón, S., et al. 2021, MNRAS, 504, 5188
Iodice, E., Arnaboldi, M., Rejkuba, M., et al. 2014, A&A, 567, A86
Jarrett, T. H. 2000, PASP, 112, 1008
Järvelä, E. 2018, Doctoral Thesis, School of Electrical Engineering, Finland
Järvelä, E., Lähteenmäki, A., & Léon-Tavares, J. 2015, A&A, 573, A76
Järvelä, E., Lähteenmäki, A., Lietzen, H., et al. 2017, A&A, 606, A9
Järvelä, E., Lähteenmäki, A., & Berton, M. 2018, A&A, 619, A69
Järvelä, E., Berton, M., & Crepaldi, L. 2021, Front. Astron. Space Sci., 8, 147
Järvelä, E., Dahale, R., Crepaldi, L., et al. 2022, A&A, 658, A12
Keel, W. C., White, R. E., I, Owen, F. N., & Ledlow, M. J. 2006, AJ, 132, 2233
Komossa, S., Voges, W., Xu, D., et al. 2006, AJ, 132, 531
Komossa, S., Xu, D., Zhou, H., Storchi-Bergmann, T., & Binette, L. 2008, ApJ, 680, 926
Kormendy, J., & Kennicutt, R. C., Jr 2004, ARA&A, 42, 603
Koss, M. J., Strittmatter, B., Lamperti, I., et al. 2021, ApJS, 252, 29
Kotilainen, J. K., León-Tavares, J., Olguín-Iglesias, A., et al. 2016, ApJ, 832, 157
Krongold, Y., Dultzin-Hacyan, D., & Marziani, P. 2001, AJ, 121, 702
Lähteenmäki, A., Järvelä, E., Hovatta, T., et al. 2017, A&A, 603, A100
Lähteenmäki, A., Järvelä, E., Ramakrishnan, V., et al. 2018, A&A, 614, L1
León Tavares, J., Kotilainen, J., Chavushyan, V., et al. 2014, ApJ, 795, 58
Marziani, P., Dultzin, D., Sulentic, J. W., et al. 2018, Front. Astron. Space Sci., 5, 6
Mathur, S. 2000, MNRAS, 314, L17
Mathur, S., Fields, D., Peterson, B. M., & Grupe, D. 2012, ApJ, 754, 146
Menéndez-Delmestre, K., Sheth, K., Schinnerer, E., Jarrett, T. H., & Scoville, N. Z. 2007, ApJ, 657, 790
Ohta, K., Aoki, K., Kawaguchi, T., & Kiuchi, G. 2007, ApJS, 169, 1
Olguín-Iglesias, A., Kotilainen, J. K., León Tavares, J., Chavushyan, V., & Añorve, C. 2017, MNRAS, 467, 3712
Olguín-Iglesias, A., Kotilainen, J., & Chavushyan, V. 2020, MNRAS, 492, 1450
Orban de Xivry, G., Davies, R., Schartmann, M., et al. 2011, MNRAS, 417, 2721
Osterbrock, D. E., & Pogge, R. W. 1985, ApJ, 297, 166
Pan, X., Zhou, H., Yang, C., et al. 2021, ApJ, 912, 118
Peng, C. Y., Ho, L. C., Impey, C. D., & Rix, H.-W. 2010, AJ, 139, 2097
Peterson, B. M. 2011, ArXiv e-prints [arXiv:1109.4181]
Salomé, Q., Longinotti, A. L., Krongold, Y., et al. 2021, MNRAS, 501, 219
Sánchez Almeida, J. 2020, MNRAS, 495, 78
Saulder, C., van Kampen, E., Chilingarian, I. V., Mieske, S., & Zeilinger, W. W. 2016, A&A, 596, A14
Sbarrato, T., Ghisellini, G., Giovannini, G., & Giroletti, M. 2021, A&A, 655, A95
Spergel, D. N., Bean, R., Doré, O., et al. 2007, ApJS, 170, 377
Stetson, P. B. 1987, PASP, 99, 191
Tortosa, A., Ricci, C., Tombesi, F., et al. 2022, MNRAS, 509, 3599
Varglund, I., Järvelä, E., Lähteenmäki, A., et al. 2022, A&A, 668, A91
Vietri, A., Järvelä, E., Berton, M., et al. 2022, A&A, 662, A20
Wang, F., Du, P., Hu, C., et al. 2016, ApJ, 824, 149
Winkel, N., Husemann, B., Davis, T. A., et al. 2022, A&A, 663, A104
Wozniak, H., Friedli, D., Martinet, L., Martin, P., & Bratschi, P. 1995, A&AS, 111, 115
Wu, Z., Ho, L. C., & Zhuang, M.-Y. 2022, ApJ, 941, 95
Yuan, W., Zhou, H. Y., Komossa, S., et al. 2008, ApJ, 685, 801
Zamanov, R., Marziani, P., Sulentic, J. W., et al. 2002, ApJ, 576, 9
Zhou, H., Wang, T., Yuan, W., et al. 2006, ApJ, 166, 128